ISSN 0915-633X

NATIONAL INSTITUTE FOR FUSION SCIENCE

Modeling of Magnetic Island Formation in Magnetic Reconnection Experiment

T.-H. Watanabe, T. Hayashi, T. Sato,
M. Yamada and H. Ji

(Received - Jan. 29, 1999)

NIFS-584 Feb. 1999

RESEARCH REPORT
NIFS Series

NAGOYA, JAPAN

Accepted for publication
in *Phys.Plasmas*

Modeling of magnetic island formation in magnetic reconnection experiment

T.-H.Watanabe, T.Hayashi, and T.Sato

Theory and Computer Simulation Center
National Institute for Fusion Science, Toki, Gifu, 509-5292, Japan

M.Yamada and H.Ji

Plasma Physics Laboratory, Princeton University, P.O.Box 451
Princeton, New Jersey 08543

Formation of a magnetic island found in the Magnetic Reconnection Experiment (MRX) (M.Yamada, H.Ji, S.Hsu, et al., Phys. Plasmas **4**, 1936 (1997)) is investigated by a magnetohydrodynamic (MHD) relaxation theory and a numerical simulation. In the co-helicity injection with a mean toroidal field, the growing process of the island into a spheromak type configuration is explained by quasi-static transition of the force-free and minimum energy state to a state with larger normalized helicity. It also turns out that no magnetic island would be generated in the counter-helicity case. The MHD simulation with inhomogeneous electric resistivity agrees with experimental results, which clearly shows formation and growth of the magnetic island in a diffusion region where the reconnection takes place.

PACS number(s): 52.30.-q, 52.30.-jb, 52.65.-y
Key words : MHD, resistive MHD, plasma simulation

I Introduction

Magnetic reconnection has been regarded as one of the most important and fundamental processes in macroscopic phenomena in fusion, space, and astrophysical plasmas[1],[2],[3]. It is accepted that reconnection produces two significant effects, namely, the topological change of field lines and the conversion of energy. In the reconnection process, the released magnetic energy is converted into kinetic and thermal energies, resulting in acceleration and heating of the plasma. The topological change of field lines allows the plasma and magnetic field to relax towards a lower energy state characterized with a different topology[4].

Recently, experimental studies of magnetic reconnection in magnetohydrodynamic (MHD) plasmas have been initiated by using coalescence of spheromaks[5], where two types of operation mode have been pursued. One is a co-helicity merging using two identical spheromaks. The another one is a counter-helicity merging where toroidal fields in spheromaks are anti-parallel. In a sequence of experiments, it was found that a field-reversed configuration (FRC) is obtained when the counter-helicity merging occurred through reconnection, whereas a spheromak is formed in the co-helicity case. An MHD simulation of the spheromak merging has confirmed the spontaneous FRC formation with effective plasma heating by magnetic reconnection[6].

In the Magnetic Reconnection Experiment (MRX)[7] reconnection is examined as an elementary process in a plasma under a controlled condition,

where a pair of flux-core (FC) coils with time-varying electric current inductively changes the field configuration to cause a plasma flow. The induced plasma flow drives the magnetic reconnection at the separatrix point (X-point). Two types of injection mode of a toroidal field (TF) are also available in the MRX, namely, co- and counter-helicity injections. Yamada and his co-workers have found O-point formation during the magnetic reconnection in the co-helicity injection of the "pull" operation mode, where poloidal field (PF) coil currents are decreased in time. The O-point formed in the reconnection region grows like a spheromak[8],[9]. In the counter-helicity case, on the other hand, a Y-shaped current sheet is formed when the magnetic reconnection takes place.

By means of MHD simulations using an adaptive mesh refinement technique, Schnack[10] has found formation of a small island during the null-helicity injection with no toroidal field, although it is unstable to motion along the current sheet and cannot grow stably.

In this paper, we report an investigation of the formation and growth mechanism of the magnetic island in the co-helicity injection of MRX. Since the MRX plasma has low temperature, its magnetic field would be approximately force-free. The Taylor state[11] in a rectangular container with a pair of FC coils is analyzed in the next section, which will suggest a plausible explanation to the island growth. Results of the MHD simulations and conclusions are given in section III and IV, respectively.

II Taylor states in MRX configuration

In this study we employ an MHD model of the MRX plasma, neglecting toroidal effects. A rectangular plasma container is taken to be a perfect conductor bounding the poloidal plasma domain of $-L_x \leq x \leq L_x$ and $-L_y \leq y \leq L_y$. We have assumed symmetry in z (toroidal) direction. Since no center rod is used in the MRX, one of the side boundaries at $x = \pm L_x$ corresponds to the major (symmetry) axis in comparison of the model configuration with the MRX device. Hereafter, we define $L_x = 1$ as a unit of length. L_y is set to be 1.4. A pair of FC coils with their radii of 0.2 are, respectively, placed at $(x, y) = (0, \pm 0.6)$. In order to accurately impose boundary conditions on the FC coils, we have used numerical grid points in generalized curvilinear coordinates as shown in Fig.1.

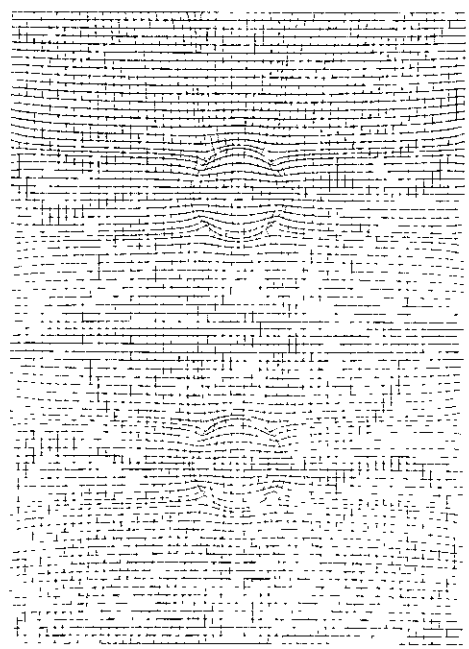

Figure 1: An example of numerical grids in generalized curvilinear coordinates used in computation.

First, we consider a case of the co-helicity injection. In a system with symmetry in z direction, a vector potential $\boldsymbol{A}$ can be given by

$$\boldsymbol{A} = \Psi \hat{z} + \nabla H \times \hat{z} \ , \qquad (1)$$

where Ψ and H are scalar functions. Ψ means the so-called poloidal flux, although Eq.(1) involves freedom of a gauge potential. The magnetic field and the current density are, respectively,

$$\boldsymbol{B} = -\nabla^2 H \hat{z} + \nabla \Psi \times \hat{z} \qquad (2)$$

and

$$\boldsymbol{j} = -\nabla^2\Psi\hat{z} - \nabla(\nabla^2 H)\times\hat{z}\ . \qquad (3)$$

Substituting Eqs.(2) and (3) into the force-free equation of the Taylor state, $\boldsymbol{j} + \mu\boldsymbol{B} = 0$, one finds that

$$\nabla^2\Psi = -\mu\nabla^2 H \qquad (4)$$

and

$$\nabla(\nabla^2 H) = \mu\nabla\Psi\ . \qquad (5)$$

Integration of Eq.(5) leads to

$$\nabla^2 H = \mu\Psi + C \qquad (6)$$

where C giving the vacuum toroidal field for $\mu = 0$ should be determined so that a constant gauge potential X cannot influence on the left hand side. In other words, for a gauge transformation of $\Psi \rightarrow \Psi + X$, C must be transformed as $C \rightarrow C - \mu X$, because $\nabla^2 H$, namely, B_z is gauge invariant. Since no external TF coil is used in the MRX device, one can choose $C = 0$ when $\Psi = 0$ on the container wall (outer boundary). It leads to

$$\nabla^2\Psi + \mu^2\Psi = 0\ . \qquad (7)$$

A boundary condition on the FC coil surfaces is given by $\Psi = \Psi_0 = constant$[12]. One may set $\Psi_0 = 1$ without loss of generality, since Ψ_0 is used just to determine the amplitude of Ψ. Let us define $\tilde{\Psi} \equiv \Psi - \Psi_v$, where the poloidal flux of a vacuum field Ψ_v is calculated from $\nabla^2\Psi_v = 0$ with $\Psi_v = 0$ and Ψ_0 on the outer and inner boundaries. Therefore, $\tilde{\Psi}$ is a solution of

$$\nabla^2\tilde{\Psi} + \mu^2\tilde{\Psi} = -\mu^2\Psi_v \qquad (8)$$

satisfying $\tilde{\Psi} = 0$ on the both boundaries. Solving Eq.(7) or (8) for given μ and Ψ_0, one finds a Taylor state in the model of MRX.

According to Taylor[13], the magnetic helicity in a torus is defined as $K = \int \boldsymbol{A}\cdot\boldsymbol{B}dv - \oint \boldsymbol{A}\cdot d\boldsymbol{l}\oint \boldsymbol{A}\cdot d\boldsymbol{s}$ so that K is indeed invariant to a multi-valued gauge potential χ. Here, $d\boldsymbol{l}$ and $d\boldsymbol{s}$ denote loop integrals the long and short way around the toroidal surface. In the model configuration of MRX, the gauge-invariant helicity is written as follows:

$$K \equiv \int \boldsymbol{A}\cdot\boldsymbol{B}dxdy - \sum_i \Psi_0 \oint \boldsymbol{A}\cdot d\boldsymbol{l}_i\ , \qquad (9)$$

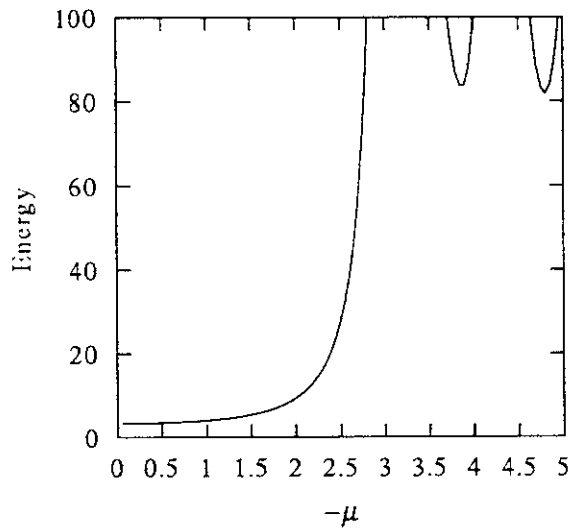

Figure 2: Magnetic energy versus μ of the Taylor state with $\Psi_0 = 1$.

where $d\boldsymbol{l}_i$ means the loop integral around the i-th FC coil surface, while $dxdy$ denotes the integral in the multiply-connected region between the outer and inner boundaries. Substituting Eqs.(1) and (2) into (9), after some manipulation using Gauss's theorem, one finds

$$K = -2\int \Psi\nabla^2 H\ dxdy \qquad (10)$$

when $\Psi = 0$ and Ψ_0 on outer and inner boundaries. Calculation of the magnetic energy E is straightforward, that is,

$$E \equiv \frac{1}{2}\int B^2 dxdy = \frac{1}{2}\int \left\{(\nabla^2 H)^2 + (\nabla\Psi)^2\right\} dxdy\ . \qquad (11)$$

We have numerically solved Eq.(7) by the second-order finite difference and the conjugate-gradient method, calculating E and K. The numerical solutions are shown in Figs.2 and 3.
Here, μ is set to be negative so that Ψ_0 and K are positive. Fig.2 shows that the energy increases with $|\mu|$, when $|\mu|$ is less than the lowest eigenvalue λ_1 of $\nabla^2 f_m + \lambda_m^2 f_m = 0$[14] ($\lambda_1 \simeq 3.2$ in the present case). This is because $\tilde{\Psi}$ satisfying

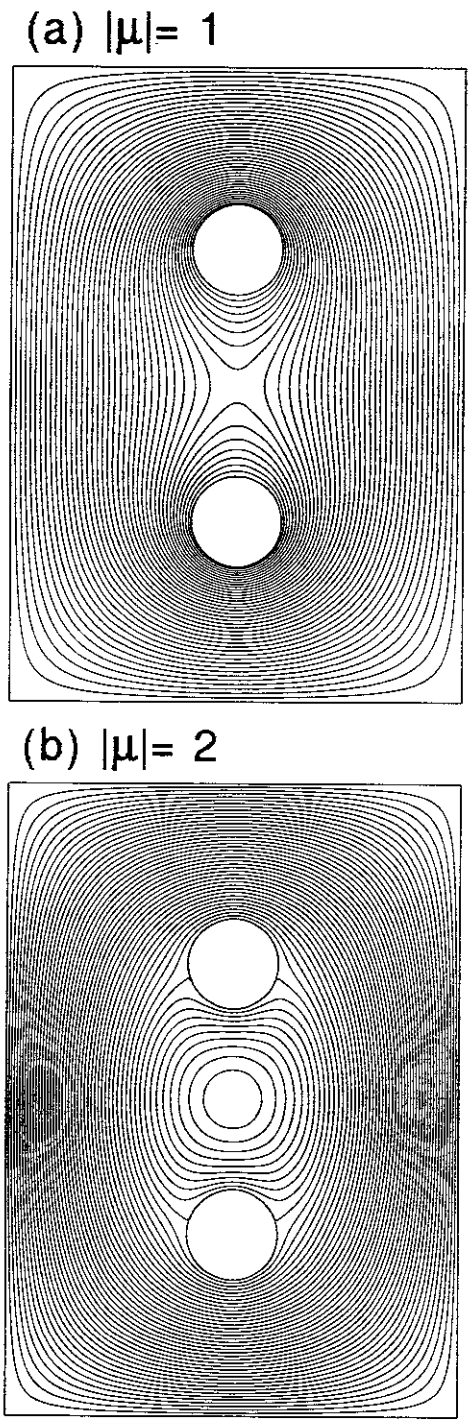

Figure 3: Contour plots of poloidal flux for (a) $|\mu| = 1$ and (b) 2.

Eq.(8) becomes much larger than Ψ_v as $|\mu|$ approaches to λ_1, where $\tilde{\Psi}$, as well as Ψ, is approximate to the lowest eigenfunction f_1. During $|\mu|$ is increased from 0 to λ_1, therefore, a magnetic island due to $\tilde{\Psi}$ appears and grows. Contour plots of Ψ for $|\mu| = 1$ and 2 in Fig.3 clearly shows a topological change of the Taylor state due to appearance of a magnetic island at the center of the system. The magnetic island becomes visible for $|\mu| > 1.6$. As $|\mu|$ approaches to λ_1 further, the island with a spheromak-like configuration grows and finally covers the whole system.

In the co-helicity injection, the MRX plasma before decreasing the PF coil current may be approximate to a solution of Eq.(7) for $|\mu| < 1.6$. As the PF coil current is reduced in a time scale longer than the Alfvén transit time, Ψ is "pulled" into the FC coils, namely, Ψ_0 becomes smaller. By short-circuiting the TF coil, toroidal flux would be conserved. This means that more plasma current is induced in the system, namely, $|\mu|$ is increased by decreasing Ψ (see Eq.(6)). Thus, the energy and helicity, respectively, normalized by $(\Psi_0/L_x)^2$ and Ψ_0^2/L_x are increased. According to the Taylor state analysis given above, therefore, when $|\mu| > 1.6$, the magnetic island will appear and grow spontaneously during the pulling operation with the co-helicity injection.

The Taylor state analysis also suggests that no magnetic island is formed in the counter-helicity injection. The reason is that, in the MRX configuration, there is no Taylor state having anti-symmetry with respect to $y = 0$. Since Ψ_v, namely, the PF current in the FC coils is assumed to be symmetric, $\tilde{\Psi}$, therefore, Ψ and B_z should be symmetric in y for $\mu \neq \lambda_m$. Extending the definition of the Taylor state with a constant μ, thus, one may consider an anti-symmetric μ profile, which has opposite signs in $y > 0$ and $y < 0$, so that B_z could be anti-symmetric for any symmetric Ψ. A possible configuration with the anti-symmetric μ is as follows: The toroidal current j_z flows only in the "private" region inside of the figure-eight separatrix magnetic surface, while $j_z = 0$, namely, $\mu = 0$ in the "public" region outside of the separatrix surface. This

is because j_z is a flux function (see Eq.(3) and (7)). Even if μ is anti-symmetric, therefore, no magnetic island with a mean toroidal current is formed in the counter-helicity case for $|\mu| < \lambda_1$.

III MHD simulation of MRX discharge

In order to check the prediction for the magnetic island formation in the last section, we have performed two-dimensional MHD simulations with the initial condition given by the Taylor state of $\mu = -1$ and $\Psi_0 = 1$, and have examined a time evolution of the system, with slowly decreasing Ψ_0 in time. Governing equations are as follows:

$$\frac{\partial \rho}{\partial t} = -\nabla \cdot (\rho \boldsymbol{v}) , \quad (12)$$

$$\rho \frac{d\boldsymbol{v}}{dt} = -\nabla p + \boldsymbol{j} \times \boldsymbol{B} + \nu(\nabla^2 \boldsymbol{v} + \frac{1}{3}\nabla(\nabla \cdot \boldsymbol{v})) , \quad (13)$$

$$\frac{dp}{dt} = -\frac{\Gamma}{p}\nabla \cdot \boldsymbol{v} + (\Gamma - 1)(\eta j^2 + \Phi) , \quad (14)$$

$$\frac{\partial \Psi}{\partial t} = -E_z , \quad (15)$$

$$\frac{\partial B_z}{\partial t} = -\nabla \times \boldsymbol{E}_p . \quad (16)$$

Here, $\boldsymbol{j}$, $\boldsymbol{E}$, $\boldsymbol{B}$, Φ and e_{ij} are, respectively, given by

$$\boldsymbol{j} = j_z \hat{\boldsymbol{z}} + \boldsymbol{j}_p = -\hat{\boldsymbol{z}}\nabla^2 \Psi + \nabla B_z \times \hat{\boldsymbol{z}} , \quad (17)$$

$$\boldsymbol{E} = E_z \hat{\boldsymbol{z}} + \boldsymbol{E}_p = -\boldsymbol{v} \times \boldsymbol{B} + \eta \boldsymbol{j} , \quad (18)$$

$$\boldsymbol{B} = B_z \hat{\boldsymbol{z}} + \nabla \Psi \times \hat{\boldsymbol{z}} , \quad (19)$$

$$\Phi = 2\nu \left(e_{ij} e_{ij} - \frac{1}{3}(\nabla \cdot \boldsymbol{v})^2 \right) , \quad (20)$$

$$e_{ij} = \frac{1}{2}\left(\frac{\partial v_i}{\partial x_j} + \frac{\partial v_j}{\partial x_i} \right) . \quad (21)$$

The suffix p denotes a poloidal (x, y) component of a vector. Velocity $\boldsymbol{v}$ is set to be zero on the boundaries. We have used a perfect conductor for the outer boundary, while $\boldsymbol{E}_p = 0$ and $E_z = 0.01$ on the inner boundaries that correspond to the FC coil surfaces. All of physical quantities are normalized by the typical length

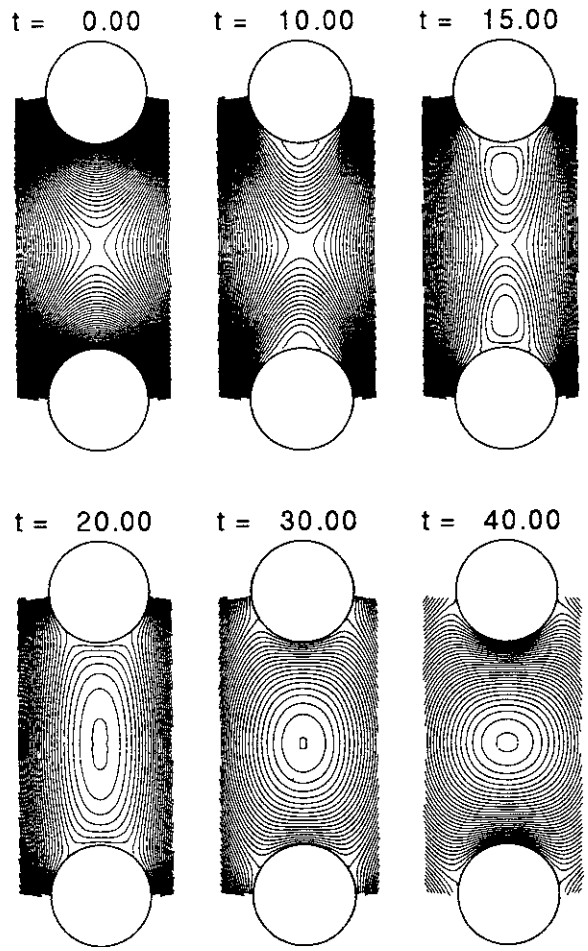

Figure 4: Contour plots of poloidal flux at different time steps in the MHD simulation with a constant resistivity ($\eta = 1 \times 10^{-3}$).

$L_x = 1$, a characteristic poloidal magnetic field $B_{p0} = \Psi_0 / L_x = 1$, and the initial density $\rho_0 = 1$. The Alfvén velocity V_{A0} given by B_{p0} and ρ_0 is equal to 1. Time is measured by the Alfvén transit time $\tau_A = L_x / V_{A0}$. The initial pressure is set to be $p = 0.2$. Viscosity ν and ratio of the specific heats Γ are, respectively, $\nu = 1 \times 10^{-3}$ and $\Gamma = 5/3$.

First, we have performed the MHD simulations with a constant resistivity η, adding infinitesimal random perturbations of $\boldsymbol{v}$ at $t = 0$. Starting from the initial condition with the

boundary condition given above, Eqs.(12)-(16) are integrated in time by the fourth-order Runge-Kutta-Gill method[15],[16]. Spatial derivatives are calculated by the second-order finite difference. Fig.4 shows contour plots of Ψ at different time steps for $\eta = 1 \times 10^{-3}$, where only an area nearby FC coils is plotted for clarity. The Lundquist number S is equal to the inverse of η, that is, 10^3 in this case. Total grid points of 101×141 including FC coils are employed in this simulation, while a convergence check using finer grid points of 201×281 gives the same results. Two circles on top and bottom of each figure represent the FC coil surfaces. Decreasing of Ψ_0 on the FC coil surfaces causes a plasma flow which drives magnetic reconnection at the X-point, while an induction current is enhanced around the FC coils. The increased current detaches a part of the "private" flux from each FC coil surface, and forms magnetic islands (see a plot at $t = 15\tau_A$). The formation process of the islands is the same as that of the S-1 spheromak using a FC coil[12],[17]. Then, the magnetic islands collide with each other, and merge into a larger one. As Ψ_0 is decreased further, the single island grows more and covers the whole system, as is predicted by the Taylor state analysis in the last section. Through several simulations with different η from 5×10^{-4} to 1×10^{-2}, we have found common features in their time evolutions, such as detachment of the "private" flux, merging of the two islands, and growth of the merged island.

In Fig.5 we have plotted the normalized magnetic energy versus the helicity resulted from the MHD simulations with $\eta = 1 \times 10^{-3}$ and 5×10^{-4}. For $\eta = 5 \times 10^{-4}$, we have used 201×281 grid points. A solid line in the figure shows the Taylor state given by Eq.(7), while marks represent the simulation results at every $5\tau_A$. Here, the energy E and helicity H are, respectively, normalized by $(\Psi_0/L_x)^2$ and Ψ_0^2/L_x. One finds that, following the Taylor state, the normalized energy and helicity are increased as Ψ_0 is decreased in time. Thus, the magnetic island appears and grows. It is also seen that the time evolution of E and H

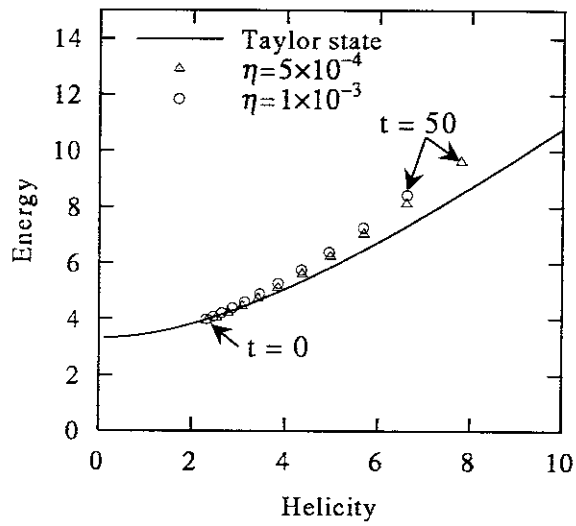

Figure 5: Evolution of the magnetic energy and helicity. Solid line shows the Taylor state. Marks representing simulation results are plotted at every $5\tau_A$.

for smaller η is closer to the Taylor state.

The above simulation result explains the growth of a magnetic island found in the MRX co-helicity discharge. In the experiment, however, the island appears in a central plasma region apart from the FC coil surfaces. Namely, it is created when a mean poloidal flux remains in the "private" regions. On the other hand, in the above simulation, two islands are formed by reconnection on the FC coil surfaces. This is because the large induction current flows around the FC coils due to the constant η. It is, however, considered that η might be larger nearby the FC coils than in the central region because of higher impurity density. Thus, we have performed simulations with an inhomogeneous η such as

$$\eta = \eta_0 \left[1 + C_\eta \exp\left\{-(r - r_c)^2/r_c^2\right\}\right] , \quad (22)$$

where r and r_c denote a distance from a center of the nearest FC coil and its radius.
In Fig.6 we show contour maps of Ψ at different time steps for $\eta_0 = 5 \times 10^{-4}$ and $C_\eta = 20$. As seen in the figures a small island appears in the cur-

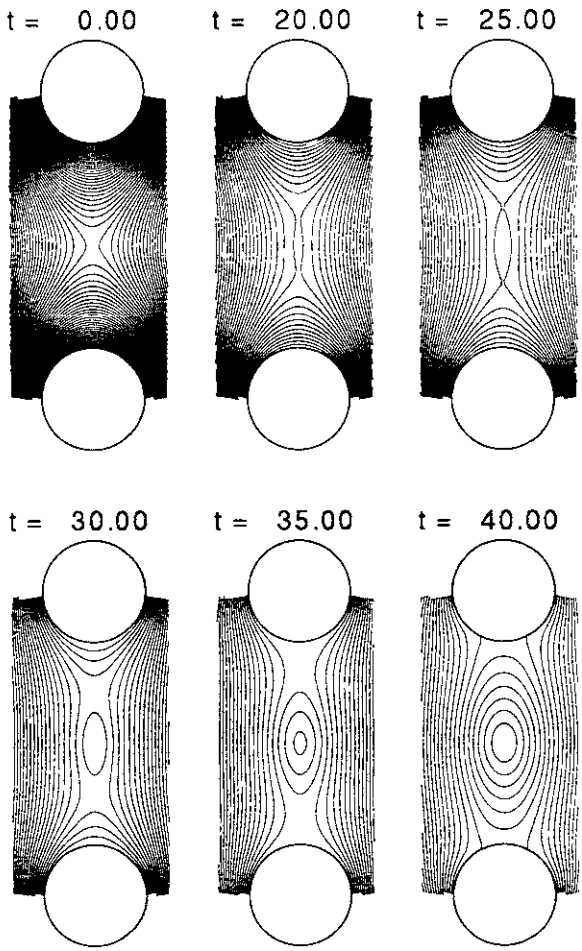

Figure 6: Same as Fig.4 but with a non-uniform resistivity.

rent layer accompanying reconnection, and gradually becomes larger while Ψ_0 is reduced. The formation process of the magnetic island is consistent with the MRX one. We have also found that the induction current mainly flows in the central region, where the island is created, rather than around the FC coils because of the inhomogeneous η profile. In addition, it is confirmed that, for smaller C_η such as $C_\eta = 10$ with $\eta_0 = 5 \times 10^{-4}$, magnetic islands appear on the FC coil surfaces as seen in Fig.4, which suggests the importance of the non-uniform η in the island formation.

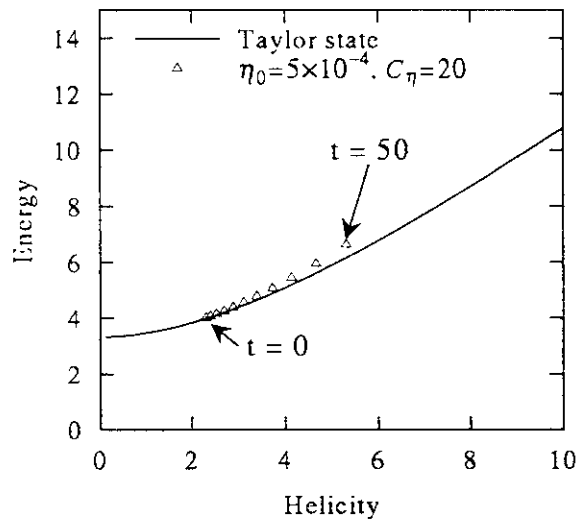

Figure 7: Same as Fig.5 but with a non-uniform resistivity.

Fig.7 shows the normalized helicity and energy obtained by the simulation in Fig.6.
Even with the larger resistivity near the FC coil surfaces, the helicity and energy are increased along the Taylor state, although the increasing rate is smaller than the constant η cases in Fig.5. Thus, it is suggested that the global property of island growth could be explained by the Taylor's theory, whereas the resistivity influences on the detail process of island formation in an early phase and its time scale.

IV Concluding remarks

In this study we have investigated the magnetic island formation in the MRX discharge. The Taylor state analysis shows that two types of solutions with and without a magnetic island belong to the lowest branch which continues from $\mu = 0$ to $|\mu| = \lambda_1$. Quasi-static transition of the field configuration along the branch can explain growth of the magnetic island during the poloidal flux is "pulled" into the FC coils, since the normalized helicity, namely, μ is increased by decreasing the PF coil currents. It is also

deduced from the Taylor state analysis that no magnetic island is formed in the counter-helicity injection. While the theoretical analysis gives an understanding on the global evolution of the system, a detailed process for appearance of the island needs a more realistic consideration, that is, the non-uniform resistivity. The inhomogeneous resistivity such as Eq.(22) enables the induction current to concentrate in the central plasma region rather than around the FC coils, and thus, to form the magnetic island apart from the coil surfaces. The simulation result using the MHD model with the non-uniform resistivity can successfully explain the co-helicity injection of MRX in the "pulling" operation mode.

Acknowledgment

One of the authors (T.-H.W.) would like to thank S.C.Jardin, R.M.Kulsrud, S.Kida, R.Horiuchi, K.Kusano and A.Kageyama for their fruitful comments and discussions. Numerical computations in this study are performed on the NIFS MISSION System (Man-Machine Interactive System for Simulation). This work is partially supported by the grants-in-aid of Ministry of Education, Science, Culture, and Sports in Japan (09780445, 10898016, 0987890, and 10044105) and the exchange program of the Joint Institute for Fusion Theory (97JF1-14).

References

[1] E.N.Paker, in *Cosmical Magnetic Fields* (Clarendon Press, Oxford, 1979).

[2] T.Sato and T.Hayashi, Phys. Fluids **22**, 1189 (1979); H.Amo. T.Sato, A.Kageyama, and the Complexity Simulation Group, Phys. Rev. E, 3838 (1995).

[3] D.Biskamp, Phys. Rep. **237**, 179 (1993).

[4] T.Sato and K.Kusano, Phys. Rev. Lett. **54**, 808 (1985).

[5] M. Yamada, Y. Ono, A. Hayakawa, M. Katsurai, and F.W. Perkins, Phys. Rev. Lett. **65**, 721 (1990).

[6] T.-H.Watanabe, T.Sato, and T.Hayashi, Phys. Plasmas **4**, 1297 (1997).

[7] M.Yamada, H.Ji, S.Hsu, T.Carter, R.Kulsrud, N.Bretz, F.Jobes, Y.Ono, and F.Perkins, Phys. Plasmas **4**, 1936 (1997).

[8] M.Yamada, H.Ji, T.A.Carter, S.C.Hsu, R.M.Kulsrud, N.L.Bretz, F.C.Jones, Y.Ono, M.Katsurai, T.-H.Watanabe, T.Sato, and T.Hayashi, in *Proceedings of the 16th International Conference on Fusion Energy*, Montreal, 1996 (International Atomic Energy Agency, Vienna, 1997), vol.2, p.253.

[9] M.Yamada, H.Ji, S.Hsu, T.Carter, R.Kulsrud, Y.Ono, and F.Perkins, Phys. Rev. Lett. **78**, 3117 (1997).

[10] D.D.Schnack, private communication (1998).

[11] J.B.Taylor, Phys. Rev. Lett. **33**, 1139 (1974).

[12] S.C.Jardin and W.Park, Phys. Fluids **24**, 679 (1981).

[13] J.B.Taylor, Rev. Mod. Phys. **58**, 741 (1986).

[14] T.H.Jensen and M.S.Chu, Phys. Fluids **27**, 2881 (1984).

[15] R.Horiuchi and T.Sato, Phys.Fluids **B1**, 581 (1989).

[16] K.Watanabe and T.Sato, J.Geophys.Res. **95**, 75 (1990).

[17] M.Yamada, H.P.Furth, W.Hsu, A.Janos, S.Jardin, M.Okabayashi, J.Sinnis, T.H.Stix, and K.Yamazaki, Phys. Rev. Lett. **46**, 188 (1981).

Recent Issues of NIFS Series

NIFS-520 S Kida and H Miura,
Identification and Analysis of Vortical Structures, Nov 1997

NIFS-521 K Ida, S Nishimura, T Minami, K Tanaka, S. Okamura, M Osakabe, H Idei, S. Kubo, C Takahashi and K. Matsuoka,
High Ion Temperature Mode in CHS Heliotron/torsatron Plasmas, Nov. 1997

NIFS-522 M. Yokoyama, N. Nakajima and M. Okamoto,
Realization and Classification of Symmetric Stellarator Configurations through Plasma Boundary Modulations, Dec 1997

NIFS-523 H Kitauchi,
Topological Structure of Magnetic Flux Lines Generated by Thermal Convection in a Rotating Spherical Shell; Dec. 1997

NIFS-524 T Ohkawa,
Tunneling Electron Trap; Dec 1997

NIFS-525 K. Itoh, S -I Itoh, M Yagi, A. Fukuyama,
Solitary Radial Electric Field Structure in Tokamak Plasmas; Dec 1997

NIFS-526 Andrey N. Lyakhov,
Alfven Instabilities in FRC Plasma, Dec 1997

NIFS-527 J. Uramoto,
Net Current Increment of negative Muonlike Particle Produced by the Electron and Positive Ion Bunch-method, Dec 1997

NIFS-528 Andrey N Lyakhov,
Comments on Electrostastic Drift Instabilities in Field Reversed Configuraiton; Dec. 1997

NIFS-529 J. Uramoto,
Pair Creation of Negative and Positive Pionlike (Muonlike) Particle by Interaction between an Electron Bunch and a Positive Ion Bunch; Dec. 1997

NIFS-530 J. Uramoto,
Measuring Method of Decay Time of Negative Muonlike Particle by Beam Collector Applied RF Bias Voltage; Dec. 1997

NIFS-531 J Uramoto,
Confirmation Method for Metal Plate Penetration of Low Energy Negative Pionlike or Muonlike Particle Beam under Positive Ions, Dec. 1997

NIFS-532 J. Uramoto,
Pair Creations of Negative and Positive Pionlike (Muonlike) Particle or K Mesonlike (Muonlike) Particle in H2 or D2 Gas Discharge in Magnetic Field, Dec 1997

NIFS-533 S. Kawata, C. Boonmee, T. Teramoto, L. Drska, J. Limpouch, R. Liska, M. Sinor,
Computer-Assisted Particle-in-Cell Code Development, Dec. 1997

NIFS-534 Y Matsukawa, T. Suda, S. Ohnuki and C. Namba,
Microstructure and Mechanical Property of Neutron Irradiated TiNi Shape Memory Alloy; Jan 1998

NIFS-535 A. Fujisawa, H. Iguchi, H. Idei, S. Kubo, K. Matsuoka, S. Okamura, K Tanaka, T. Minami, S. Ohdachi, S. Morita, H. Zushi, S. Lee, M. Osakabe, R Akiyama, Y Yoshimura, K. Toi, H. Sanuki, K Itoh, A. Shimizu, S. Takagi, A Ejiri, C Takahashi, M. Kojima, S. Hidekuma, K. Ida, S. Nishimura, N. Inoue, R. Sakamoto, S.-I Itoh, Y Hamada, M Fujiwara,
Discovery of Electric Pulsation in a Toroidal Helical Plasma; Jan 1998

NIFS-536 Lj.R. Hadzievski, M.M. Skoric, M. Kono and T. Sato,
Simulation of Weak and Strong Langmuir Collapse Regimes; Jan. 1998

NIFS-537 H. Sugama, W. Horton,
Nonlinear Electromagnetic Gyrokinetic Equation for Plasmas with Large Mean Flows; Feb. 1998

NIFS-538 H. Iguchi, T P. Crowley, A Fujisawa, S. Lee, K. Tanaka, T. Minami, S. Nishimura, K. Ida, R. Akiyama, Y Hamada, H., Idei M.

Isobe, M. Kojima, S. Kubo, S Morita, S. Ohdachi, S Okamura, M. Osakabe, K. Matsuoka, C. Takahashi and K. Toi,
Space Potential Fluctuations during MHD Activities in the Compact Helical System (CHS); Feb 1998

NIFS-539 Takashi Yabe and Yan Zhang,
Effect of Ambient Gas on Three-Dimensional Breakup in Coronet Formation Process; Feb. 1998

NIFS-540 H Nakamura, K. Ikeda and S. Yamaguchi,
Transport Coefficients of InSb in a Strong Magnetic Field; Feb. 1998

NIFS-541 J. Uramoto,
Development of ν_μ Beam Detector and Large Area ν_μ Beam Source by H_2 Gas Discharge (I); Mar. 1998

NIFS-542 J. Uramoto,
Development of $bar\{\nu\}_\mu$ Beam Detector and Large Area $bar\{\nu\}_\mu$ Beam Source by H_2 Gas Discharge (II); Mar. 1998

NIFS-543 J. Uramoto,
Some Problems inside a Mass Analyzer for Pions Extracted from a H_2 Gas Discharge; Mar. 1998

NIFS-544 J. Uramoto,
Simplified ν_μ $bar\{\nu\}_\mu$ Beam Detector and ν_μ $bar\{\nu\}_\mu$ Beam Source by Interaction between an Electron Bunch and a Positive Ion Bunch; Mar. 1998

NIFS-545 J. Uramoto,
Various Neutrino Beams Generated by D_2 Gas Discharge; Mar 1998

NIFS-546 R. Kanno, N Nakajima, T. Hayashi and M. Okamoto,
Computational Study of Three Dimensional Equilibria with the Bootstrap Current; Mar. 1998

NIFS-547 R. Kanno, N. Nakajima and M. Okamoto,
Electron Heat Transport in a Self-Similar Structure of Magnetic Islands; Apr. 1998

NIFS-548 J.E. Rice,
Simulated Impurity Transport in LHD from MIST; May 1998

NIFS-549 M.M. Skoric, T. Sato, A.M. Maluckov and M.S. Jovanovic,
On Kinetic Complexity in a Three-Wave Interaction; June 1998

NIFS-550 S. Goto and S. Kida,
Passive Saclar Spectrum in Isotropic Turbulence: Prediction by the Lagrangian Direct-interaction Approximation; June 1998

NIFS-551 T. Kuroda, H. Sugama, R. Kanno, M. Okamoto and W. Horton,
Initial Value Problem of the Toroidal Ion Temperature Gradient Mode ; June 1998

NIFS-552 T. Mutoh, R Kumazawa, T. Seki, F. Simpo, G. Nomura, T Ido and T. Watari,
Steady State Tests of High Voltage Ceramic Feedthoughs and Co-Axial Transmission Line of ICRF Heating System for the Large Helical Device ; June 1998

NIFS-553 N. Noda, K. Tsuzuki, A. Sagara, N. Inoue, T. Muroga,
oronaization in Future Devices -Protecting Layer against Tritium and Energetic Neutrals-: July 1998

NIFS-554 S. Murakami and H Saleem,
Electromagnetic Effects on Rippling Instability and Tokamak Edge Fluctuations; July 1998

NIFS-555 H. Nakamura , K. Ikeda and S. Yamaguchi,
Physical Model of Nernst Element; Aug. 1998

NIFS-556 H Okumura, S. Yamaguchi, H. Nakamura, K. Ikeda and K. Sawada,
Numerical Computation of Thermoelectric and Thermomagnetic Effects; Aug. 1998

NIFS-557 Y. Takeiri, M. Osakabe, K. Tsumori, Y. Oka, O. Kaneko, E. Asano, T. Kawamoto, R. Akiyama and M. Tanaka,

Development of a High-Current Hydrogen-Negative Ion Source for LHD-NBI System. Aug 1998

NIFS-558 M Tanaka, A Yu Grosberg and T Tanaka,
Molecular Dynamics of Structure Organization of Polyampholytes, Sep 1998

NIFS-559 R Horiuchi, K Nishimura and T Watanabe,
Kinetic Stabilization of Tilt Disruption in Field-Reversed Configurations Sep 1998
(IAEA-CN-69/THP1/11)

NIFS-560 S. Sudo, K. Kholopenkov, K. Matsuoka, S Okamura, C Takahashi, R Akiyama, A Fujisawa, K Ida, H Idei, H. Iguchi, M Isobe, S Kado, K Kondo, S Kubo, H Kuramoto, T Minami, S Morita, S Nishimura, M Osakabe, M Sasao, B Peterson, K. Tanaka, K Toi and Y Yoshimura,
Particle Transport Study with Tracer-Encapsulated Solid Pellet Injection, Oct 1998
(IAEA-CN-69/EXP1/18)

NIFS-561 A Fujisawa, H Iguchi, S Lee, K. Tanaka, T Minami, Y. Yoshimura, M Osakabe, K Matsuoka, S Okamura, H Idei, S Kubo, S Ohdachi, S Morita, R Akiyama, K Toi, H Sanuki, K Itoh, K Ida, A Shimizu, S Takagi, C Takahashi, M Kojima, S. Hidekuma, S. Nishimura, M Isobe, A Ejiri, N Inoue, R Sakamoto, Y. Hamada and M Fujiwara,
Dynamic Behavior Associated with Electric Field Transitions in CHS Heliotron/Torsatron, Oct 1998
(IAEA-CN-69/EX5/1)

NIFS-562 S Yoshikawa,
Next Generation Toroidal Devices, Oct 1998

NIFS-563 Y. Todo and T Sato,
Kinetic-Magnetohydrodynamic Simulation Study of Fast Ions and Toroidal Alfvén Eigenmodes, Oct 1998
(IAEA-CN-69/THP2/22)

NIFS-564 T. Watari, T Shimozuma, Y. Takeiri, R Kumazawa, T Mutoh, M Sato, O. Kaneko, K. Ohkubo, S Kubo, H Idei, Y Oka, M. Osakabe, T. Seki, K. Tsumori, Y Yoshimura, R. Akiyama, T. Kawamoto, S. Kobayashi, F Shimpo, Y Takita, E. Asano, S. Itoh, G Nomura, T. Ido, M. Hamabe, M Fujiwara, A Iiyoshi, S Morimoto, T Bigelow and Y.P. Zhao,
Steady State Heating Technology Development for LHD, Oct. 1998
(IAEA-CN-69/FTP/21)

NIFS-565 A. Sagara, K Y. Watanabe, K. Yamazaki, O. Motojima, M. Fujiwara, O Mitarai, S. Imagawa, H. Yamanishi, H Chikaraishi, A. Kohyama, H. Matsui, T Muroga, T Noda, N. Ohyabu, T Satow, A.A. Shishkin, S. Tanaka, T. Terai and T Uda,
LHD-Type Compact Helical Reactors; Oct 1998
(IAEA-CN-69/FTP/03(R)

NIFS-566 N. Nakajima, J Chen, K. Ichiguchi and M. Okamoto,
Global Mode Analysis of Ideal MHD Modes in L=2 Heliotron/Torsatron Systems; Oct 1998
(IAEA-CN-69/THP1/08)

NIFS-567 K. Ida, M. Osakabe, K. Tanaka, T Minami, S Nishimura, S. Okamura, A. Fujisawa, Y. Yoshimura, S Kubo, R Akiyama, D S.Darrow, H. Idei, H. Iguchi, M Isobe, S. Kado, T Kondo, S. Lee, K Matsuoka, S Morita, I Nomura, S Ohdachi, M. Sasao, A. Shimizu, K. Tumori, S. Takayama, M Takechi, S Takagi, C Takahashi, K Toi and T. Watari,
Transition from L Mode to High Ion Temperature Mode in CHS Heliotron/Torsatron Plasmas, Oct 1998
(IAEA-CN-69/EX2/2)

NIFS-568 S. Okamura, K Matsuoka, R Akiyama, D.S Darrow, A Ejiri, A. Fujisawa, M. Fujiwara, M Goto, K Ida H. Idei, H. Iguchi, N. Inoue, M. Isobe, K Itoh, S. Kado, K. Kholopenkov, T Kondo, S Kubo, A Lazaros, S. Lee, G. Matsunaga, T Minami, S. Morita, S. Murakami, N. Nakajima, N. Nikai, S. Nishimura, I. Nomura, S. Ohdachi, K. Ohkuni, M. Osakabe, R. Pavlichenko, B. Peterson, R. Sakamoto, H. Sanuki, M Sasao, A. Shimizu, Y Shirai, S. Sudo, S. Takagi, C Takahashi, S. Takayama, M Takechi, K Tanaka, K Toi, K. Yamazaki, Y Yoshimura and T Watari,
Confinement Physics Study in a Small Low-Aspect-Ratio Helical Device CHS, Oct 1998
(IAEA-CN-69/OV4/5)

NIFS-569 M.M. Skonc, T Sato, A. Maluckov, M.S. Jovanovic,
Micro- and Macro-scale Self-organization in a Dissipative Plasma, Oct 1998

NIFS-570 T. Hayashi, N. Mizuguchi, T-H Watanabe, T Sato and the Complexity Simulation Group,
Nonlinear Simulations of Internal Reconnection Event in Spherical Tokamak; Oct 1998
(IAEA-CN-69/TH3/3)

NIFS-571 A. Iiyoshi, A. Komori, A. Ejiri, M Emoto, H. Funaba, M. Goto, K Ida, H Idei, S Inagaki, S Kado, O Kaneko, K Kawahata, S Kubo, R Kumazawa, S. Masuzaki, T Minami, J. Miyazawa, T Morisaki, S Morita, S Murakami, S Muto, T Muto, Y Nagayama, Y. Nakamura, H. Nakanishi, K Nanhara, K Nishimura, N Noda, T Kobuchi, S Ohdachi, N. Ohyabu, Y. Oka, M. Osakabe, T Ozaki, B.J Peterson, A. Sagara, S Sakakibara, R Sakamoto, H Sasao, M Sasao, K Sato, M Sato, T. Seki, T Shimozuma, M Shoji, H. Suzuki, Y. Takeiri, K Tanaka, K. Toi, T Tokuzawa, K Tsumori, I Yamada, H Yamada, S Yamaguchi, M Yokoyama, K Y.Watanabe, T Watari, R Akiyama, H Chikaraishi, K Haba, S Hamaguchi, S Iima, S Imagawa, N Inoue, K. Iwamoto, S Kitagawa, Y. Kubota, J. Kodaira, R Maekawa, T Mito, T Nagasaka, A Nishimura, Y Takita, C Takahashi, K Takahata, K. Yamauchi, H Tamura, T Tsuzuki, S. Yamada, N Yanagi, H Yonezu, Y Hamada, K. Matsuoka, K. Murai, K. Ohkubo, I. Ohtake,

M. Okamoto, S Sato, T. Satow, S Sudo, S. Tanahashi, K. Yamazaki, M. Fujiwara and O. Motojima,
An Overview of the Large Helical Device Project; Oct. 1998
(IAEA-CN-69/OV1/4)

NIFS-572 M. Fujiwara, H. Yamada, A. Ejiri, M. Emoto, H. Funaba, M. Goto, K. Ida, H. Idei, S. Inagaki, S. Kado, O. Kaneko, K. Kawahata, A. Komori, S. Kubo, R. Kumazawa, S. Masuzaki, T. Minami, J. Miyazawa, T. Morisaki, S. Morita, S. Murakami, S. Muto, T. Muto, Y. Nagayama, Y. Nakamura, H. Nakanishi, K. Narihara, K. Nishimura, N. Noda, T. Kobuchi, S Ohdachi, N. Ohyabu, Y. Oka, M. Osakabe, T. Ozaki, B. J. Peterson, A. Sagara, S. Sakakibara, R. Sakamoto, H. Sasao, M. Sasao, K. Sato, M. Sato, T. Seki, T. Shimozuma, M. Shoji, H. Sazuki, Y. Takeiri, K. Tanaka, K. Toi, T. Tokuzawa, K. Tsumori, I. Yamada, S. Yamaguchi, M. Yokoyama, K.Y. Watanabe, T. Watari, R. Akiyama, H. Chikaraishi, K. Haba, S. Hamaguchi, M. Iima, S. Imagawa, N. Inoue, K. Iwamoto, S. Kitagawa, Y. Kubota, J. Kodaira, R. Maekawa, T. Mito, T. Nagasaka, A. Nishimura, Y. Takita, C. Takahashi, K. Takahata, K. Yamauchi, H. Tamura, T Tsuzuki, S. Yamada, N. Yanagi, H Yonezu, Y. Hamada, K. Matsuoka, K. Murai, K. Ohkubo, I. Ohtake, M. Okamoto, S. Sato, T. Satow, S. Sudo, S. Tanahashi, K. Yamazaki, O. Motojima and A. Iiyoshi,
Plasma Confinement Studies in LHD; Oct. 1998
(IAEA-CN-69/EX2/3)

NIFS-573 O. Motojima, K. Akaishi, H. Chikaraishi, H. Funaba, S. Hamaguchi, S. Imagawa, S. Inagaki, N. Inoue, A. Iwamoto, S Kitagawa, A. Komori, Y Kubota, R Maekawa, S Masuzaki, T. Mito, J Miyazawa, T Morisaki, T. Muroga, T Nagasaka, Y. Nakmura, A. Nishimura, K. Nishimura, N. Noda, N. Ohyabu, S. Sagara, S. Sakakibara, R. Sakamoto, S. Satoh, T Satow, M Shoji, H Suzuki, K. Takahata, H. Tamura, K. Watanabe, H. Yamada, S. Yamada, S. Yamaguchi, K. Yamazaki, N. Yanagi, T. Baba, H. Hayashi, M. Iima, T. Inoue, S. Kato, T. Kato, T. Kondo, S. Moriuchi, H. Ogawa, I. Ohtake, K. Ooba, H. Sekiguchi, N. Suzuki, S. Takami, Y. Taniguchi, T. Tsuzuki, N. Yamamoto, K. Yasui, H. Yonezu, M. Fujiwara and A. Iiyoshi,
Progress Summary of LHD Engineering Design and Construction; Oct. 1998
(IAEA-CN-69/FT2/1)

NIFS-574 K. Toi, M. Takechi, S. Takagi, G. Matsunaga, M. Isobe, T Kondo, M. Sasao, D.S Darrow, K. Ohkuni, S. Ohdachi, R. Akiyama A. Fujisawa, M. Gotoh, H. Idei, K. Ida, H. Iguchi, S. Kado, M Kojima, S. Kubo, S. Lee, K. Matsuoka, T Minami, S Monta, N. Nikai, S. Nishimura, S. Okamura, M. Osakabe, A. Shimizu, Y. Shirai, C Takahashi, K. Tanaka, T. Watari and Y Yoshimura,
Global MHD Modes Excited by Energetic Ions in Heliotron/Torsatron Plasmas, Oct 1998
(IAEA-CN-69/EXP1/19)

NIFS-575 Y. Hamada, A. Nishizawa, Y Kawasumi, A. Fujisawa, M. Kojima, K. Narihara, K. Ida, A. Ejiri, S Ohdachi, K. Kawahata, K Toi, K. Sato, T. Seki, H. Iguchi, K. Adachi, S. Hidekuma, S.Hirokura, K. Iwasaki, T. Ido, R. Kumazawa, H. Kuramoto, T. Minami, I.. Nomura, M. Sasao, K.N. Sato, T. Tsuzuki, I. Yamada and T. Watari,
Potential Turbulence in Tokamak Plasmas; Oct. 1998
(IAEA-CN-69/EXP2/14)

NIFS-576 S. Murakami, U. Gasparino, H. Idei, S. Kubo, H Maassberg, N. Marushchenko, N. Nakajima, M. Romé and M Okamoto,
5D Simulation Study of Suprathermal Electron Transport in Non-Axisymmetric Plasmas; Oct. 1998
(IAEA-CN-69/THP1/01)

NIFS-577 S. Fujiwara and T. Sato,
Molecular Dynamics Simulation of Structure Formation of Short Chain Molecules; Nov. 1998

NIFS-578 T. Yamagishi,
Eigenfunctions for Vlasov Equation in Multi-species Plasmas Nov. 1998

NIFS-579 M. Tanaka, A. Yu Grosberg and T. Tanaka,
Molecular Dynamics of Strongly-Coupled Multichain Coulomb Polymers in Pure and Salt Aqueous Solutions; Nov. 1998

NIFS-580 J. Chen, N. Nakajima and M. Okamoto,
Global Mode Analysis of Ideal MHD Modes in a Heliotron/Torsatron System: I. Mercier-unstable Equilibria; Dec. 1998

NIFS-581 M. Tanaka, A. Yu Grosberg and T. Tanaka,
Comparison of Multichain Coulomb Polymers in Isolated and Periodic Systems: Molecular Dynamics Study; Jan. 1999

NIFS-582 V.S. Chan and S. Murakami,
Self-Consistent Electric Field Effect on Electron Transport of ECH Plasmas; Feb. 1999

NIFS-583 M. Yokoyama, N. Nakajima, M. Okamoto, Y. Nakamura and M. Wakatani,
Roles of Bumpy Field on Collisionless Particle Confinement in Helical-Axis Heliotrons; Feb. 1999

NIFS-584 T.-H. Watanabe, T. Hayashi, T. Sato, M. Yamada and H. Ji,
Modeling of Magnetic Island Formation in Magnetic Reconnection Experiment, Feb. 1999